

Advanced Techniques for Evaluating Vulnerability of Urban Infrastructure by Integrating Multiple Evaluation Indexes

Masayoshi NAKASHIMA, Hitoshi TANAKA, Tomotaka IWATA,
Sumio SAWADA, and Shuji TAMURA

Synopsis

It is essential for disaster prevention to quantify the earthquake vulnerability of urban infrastructures in consideration of their life cycle. As part of a five-year study on this subject, presented in this article are: the refinement of prediction of strong motions, examinations into actual performance of nonstructural components, rational evaluation of RC building structures in consideration of foundation-structure interaction, effects of total earth pressure on pile forces, and development of a systematic procedure for the estimation of life-cycle cost for large-scale lifeline network. Development of a sloshing reduction damper which consists of separation wall with slits installed in cylindrical tank.

Keywords: strong ground motion, performance of nonstructural components, foundation-structure interaction, earth pressure, sloshing reduction damper

1. Introduction

The rational evaluation of earthquake vulnerability of our urban infrastructures require accurate prediction of strong motions, thorough characterization of the performance of structures, soils, structure-building system, and soil-structure systems, and development of methodologies that can effectively consider the life-cycle cost/performance of the structures and systems. This is a five-year project being undertaken within the scope of Center of Excellence for Natural Disaster Science and Disaster Reduction, implemented by the Disaster Prevention Research Institute, Kyoto University. Achievement of fiscal 2006 and five-years is summarized in what follows.

2. Strong Ground Motion Prediction for Design Ground Motion

2.1 Long-period ground motion prediction during the hypothetical Tonankai earthquake

At 19:07 and 23:57 on 5 September 2004, an

MJMA7.1 and a MJMA7.4 earthquakes occurred in the south east off the Kii peninsula, Japan, that were named the 2004 Kii-Hanto-Nanto-Okii earthquake.

These earthquakes and their aftershocks are thought to be intraplate earthquakes, which occurred in the subducting Philippine Sea Plate (The Headquarters for Earthquake Research Promotion, hereafter HERP, 2004), that was neighbor of source region of the hypothetical Tonankai earthquake. In order to estimate ground motions during the hypothetical Tonankai earthquake, we used one of aftershock events using the empirical Green's function (EGF) method by Irikura (1986). First, we determine the source size and the stress drop of the EGF event using comparison of the aftershock and the pre-event records. Those parameters were determined as 28.1 km² and 3.3 Mpa (Suzuki *et al.*, 2005). Using this event as the EGF again, we anticipated the hypothetical Tonankai earthquake and simulated the resultant strong ground motions. Although the type of earthquake was different, the focal mechanism of the EGF event acceptably

resembled that of the hypothetical Tonankai earthquake. We followed Model 2 used in HERP (2001b). This model consists of three asperities and gives a larger stress drop on the smaller asperities, as shown in Fig. 1. We only characterized the asperity portion, and ignored the background off-asperity area. The rupture starts from off the Kii peninsula and propagates in a north-easterly direction. We calculated the acceleration, velocity, and displacement waveforms predicted at the stations K-NET, KiK-net, and CEORKA, where the records of the EGF event were available. The frequency band used for this simulation was 0.05–20.0Hz. The rupture velocity was assumed to be 2.7 km/s, referring to HERP (2001b).

Figure 2 shows the distribution of seismic intensity (JMA, 1996) calculated from simulated acceleration waveforms. This is consistent with that calculated by HERP (2001b), which used the stochastic Green's function method. Large seismic intensities of more than 5+ were predicted for the Aichi and Mie prefectures, which is located toward the rupture propagation. Examples of the velocity waveforms for the stations in the Aichi and Mie prefectures (AIC016 and MIE003) and the Osaka basin (FKS and AMA) are shown in Fig. 3. At the stations such as FKS and AMA, that is in the Osaka basin, long-period ground motions last for more than 3min. Although seismic intensity in the Osaka basin is up to 5+, such long period about 3 to 6 second ground motions will hit the Osaka basin site during the Tonankai earthquake. Predominant period of predicted ground motions at the stations in the Osaka basin is different at the sites and that indicates the complex three-dimensional basin underground structure affects such the ground motion characteristics. Especially, the sites at the Osaka bay area have longer period ground motions and there are many long period structures such as high rise buildings and fuel tanks. It is necessary to consider long period ground motions during the large subduction earthquakes to reduce the seismic disaster against long period seismic waves.

At MIE003, long-duration ground motions are also observed after the direct *S*-wave. On the other hand, the waveform predicted at AIC016 mainly contains a high frequency component with very large amplitude. Seismic intensity 7 was predicted for this station. The depth to the bedrock at MIE003 is deeper than that at AIC016, although both stations are located in the Nobi

basin. That is also indicated that the complexity of the underground structure of the Nobi basin. Construction of the large basin underground velocity structure are needed.

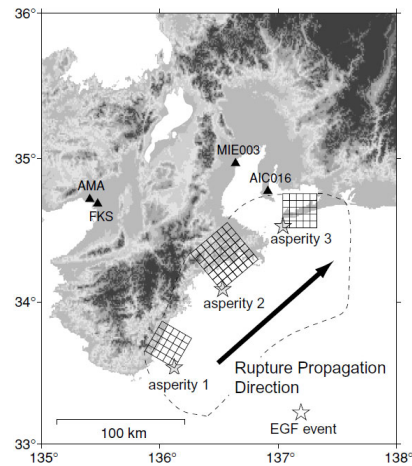


Fig.1 Source model of the hypothetical Tonankai earthquake used in this study. Each star indicates the rupture starting point of each asperity.

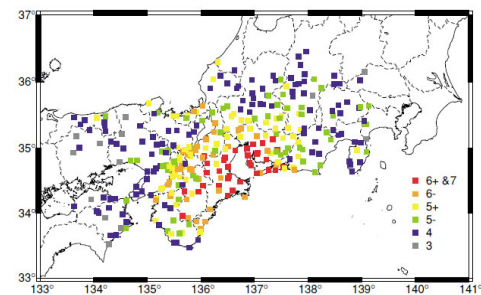


Fig. 2: Distribution of the calculated seismic intensity.

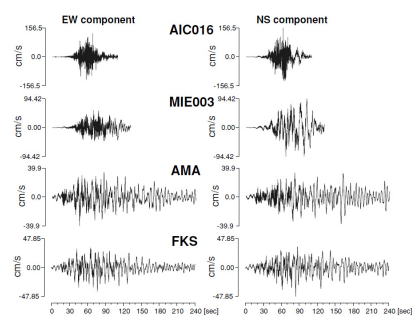


Fig. 3. Example of horizontal velocity waveforms predicted for the stations in the Aichi and Mie prefectures (AIC016 and MIE003) and in the Osaka basin (AMA and FKS).

2.2 Ground motion modeling of the 2005 Miyagi-Oki earthquake

We estimate the source model of the 2005 Miyagi-Oki earthquake, which consists of two strong

motion generation areas (SMGAs). The location of the first SMGA is determined from the arrival time differences between the first motion and the first pulse in the P-wave portion. Based on the broadband waveform modeling, we estimate the two SMGA parameters by using the empirical Green's function method. The estimated location of the two SMGAs coincides with the two major large slip areas inferred from the inversion of strong motion and teleseismic waveforms as shown in Fig. 4. It implies that the broadband strong motion, including the high-frequency range of the 2005 Miyagi-Oki earthquake, is mainly radiated from the asperities. The deeper SMGA has a larger stress drop (34.1 MPa) than the shallower SMGA (17.6 MPa).

In Fig. 5, we compare the SMGAs of the 2005 event and those of the 1978 event estimated by Kamae et al.(2002). Even using the newly-determined hypocenters by Okada et al.(2005), SMGAs of both events do not overlap each other.

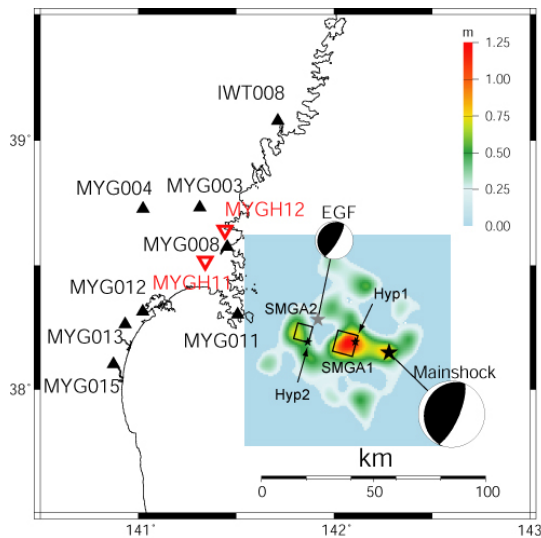


Fig. 4. The location of the estimated SMGAs projected on the slip distribution inferred by Wu and Koketsu (2005) by using strong-motion and teleseismic data, together with the strong motion stations using waveform modeling. The slip distribution is shifted to match the epicenter used in their study to that determined by the JMA or Hyp0.

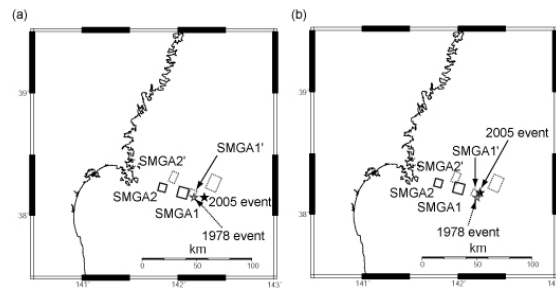


Fig. 5. Comparison of the SMGA location of the 2005 Miyagi-Oki earthquake with that of the 1978 earthquake estimated by Kamae (2006). The solid squares are the SMGAs of the 2005 event, and the dotted rectangles are those of the 2002 event. (a) The hypocenters determined by the JMA are used as reference points. (b) The distribution is shifted to adjust the hypocenters to those determined by Okada et al. (2005).

3 Performance of Nonstructural Components in Earthquake Conditions

3.1 Importance of nonstructural components in seismic design

Most research on the behavior of building structures during an earthquake only focuses on the lateral force resisting system. However, nonstructural elements also play a critical role in the performance of a structure as damage to these systems can result in significant economic losses or loss of life. In order to address this issue, this study characterizes the behavior of both nonstructural partition walls and hanging ceiling systems using the shake table at the Disaster Prevention Research Institute of Kyoto University. The test setup allowed for the interaction between perpendicular walls and the hanging ceiling system to be considered.

3.2 Test setup and specimens

In order to perform the shake table study of the nonstructural partition walls and hanging ceiling systems, a steel frame is designed to provide a means of imparting inertial loads to the system with the mass placed at the top of the loading frame. The loading frame is designed such that it will have minimal effect on the behavior of the non-structural system. Fig. 6(a) provides a view of the loading frame.

Two nonstructural specimens are tested as part of this study. Both specimens have the same nonstructural

partition wall design with the difference between them being the design of the hanging ceiling system (traditional and seismic). The nonstructural partition walls are typical gypsum board and light gage steel construction used for Japanese high-rise office structures. Further details in regards to the construction of these systems can be found in Lee et al. (2007). The partition walls are constructed on four sides so that the effects associated with perpendicular walls can be studied. The walls span 3.35 m in the long direction (X-direction) and 1.35 m in the short direction (Y-direction). In the X-direction, a door is framed into one of the walls, while the other wall has a 1.5 m wide opening. The two short direction walls are solid. The partition walls can be seen in Fig. 6(b).



(a)



(b)

Fig. 6 Test Setup: (a) Bare loading frame; (b) nonstructural specimen.

The traditional hanging ceiling uses evenly spaced threaded rods and clips to hold the ceiling, and the ceiling itself abuts up against the partition walls. The seismic ceiling uses light gage steel angles to form a truss system to further stabilize the ceiling. A gap is also left between the ceiling and the partition walls. The seismic ceiling is designed for drift levels of 1/100 radians. Figs. 7 and 8 contain pictures of the two ceiling systems.

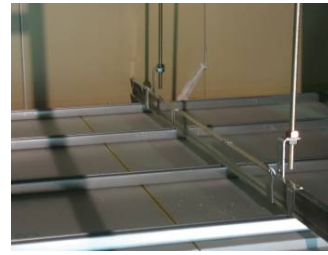


Fig. 7 Traditional hanging ceiling

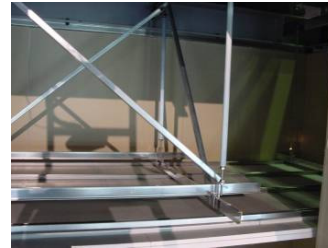


Fig. 8 Seismic hanging ceiling

The systems are loaded using a sinusoidal motion that increases in frequency during its duration. The magnitude of the acceleration of the sinusoidal motion is determined so as to apply maximum drifts of 1/200, 1/100, 1/66, 1/50 (or 1/35), and 1/28 radians with each subsequent run. At each drift level, the motion is applied in the X-direction and Y-direction separately.

3.3 Observed damage to system

Damage to the nonstructural partition walls and hanging ceiling systems are observed after each drift level to correlate the damage with drift. During loading, the nonstructural partition walls undergo a rocking behavior as a result of each of the presence of perpendicular walls. This rocking behavior results in early damage occurring at the corner of the walls. At 1/100 radians, a gap between the door frame and gypsum board formed. At a drift of 1/66 radians the door became difficult to open. Larger drift levels of 1/50 radians resulted in the screws pulling through the gypsum board minimizing the attachment to the metal studs. Cracks also began to propagate in the gypsum board from the upper corners of the doorway. Some of the gypsum board panels become detached at drift levels of 1/28 radians.

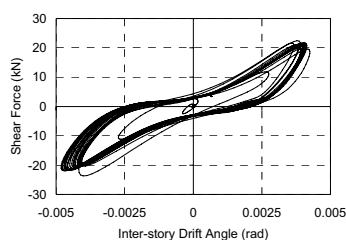
The traditional hanging ceiling systems performed well at all drift levels. The seismic hanging ceiling system also performed well up to its design drift of 1/100 radians. However, at drift levels of 1/66 radians, pounding between the ceiling and walls began to occur resulting in some of the clips between the truss system

and ceiling being dislodged. All of these clips are lost at drift levels of 1/28 radians reducing the ceiling to a more traditional configuration, but the ceiling itself remained basically undamaged.

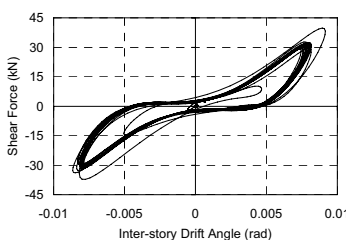
3.4 Partition wall behavior

The behavior of the nonstructural partition walls is evaluated using the shear force sustained by the non-structural system versus drift curves when loaded in the X-direction. In general, both specimens showed similar behavior. The hysteretic curves for the 1/200, 1/100, and 1/66 radian drift levels are shown in Fig. 9. The hysteretic curves show some general trends including nonlinearity of the hysteresis, stiffness and strength degradation with continued cycling, and pinching of the hysteresis with increasing drift levels. The shear force reaches a maximum value of 46 kN at the 1/35 radian drift level.

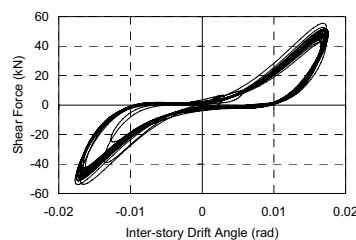
The stiffness and damping associated with this hysteretic behavior is also considered. From Fig. 9, it can be seen that the initial stiffness decreases with an increase in drift level as the system sustains damage. The secant stiffness also shows a similar decrease from 1.33 kN/mm to 0.23 kN/mm between the 1/200 radian and 1/28 radian drift cases. The change in energy dissipation based on the area enclosed by the hysteretic curve follows a similar trend as the shear force with the maximum value of 3349 kN-mm occurring during the 1/35 radian drift case.



(a)



(b)



(c)

Fig. 9. Shear versus drift behavior for the nonstructural partition walls: (a) 1/200 drift; (b) 1/100 drift; and (c) 1/66 drift.

3.5 Hanging ceiling system behavior

The traditional and seismic hanging ceiling systems are evaluated by comparing the measured ceiling acceleration to the acceleration at the top of the loading frame. For both types of ceiling systems, the values remained similar up to drift levels of 1/66 radians, since no significant damage is sustained. At the drift level of 1/28 radians, the traditional ceiling system has accelerations 25% below that of the loading frame, while the seismic ceiling systems' accelerations are 1.5 times that of the loading frame. The difference can be attributed to the gap associated with the seismic ceiling, which resulted in pounding between the ceiling and wall. The maximum accelerations sustained by the traditional ceiling system and seismic ceiling system are 1.3g (1/35 radians) and 2.9g (1/28 radians), respectively.

3.6 Conclusion

- 1) Nonstructural partition wall systems containing perpendicular walls tend to be dominated by a rocking behavior during loading.
- 2) The door system undergoes permanent damage and decreased functionality at drift levels of 1/66 radians and drift levels of 1/28 radians cause falling debris from the wall systems.
- 3) Both ceiling systems sustain minimal damage up to their intended design level with the traditional system resulting in smaller maximum accelerations.

4 Experimental Study on seismic resisting mechanisms

4.1 Lateral Force Resisting Mechanism of a Multi-Story Shear Wall and Peripheral Members

(1) Introduction

In current design procedures [RC design code:AIJ:1999] [Paulay1992], cantilever structural walls are normally assumed to stand on a solid foundation, and foundation beams, slabs and piles are designed separately without considering their interactions. This study aims to experimentally clarify the variation of the lateral load resisting mechanisms considering the interaction between a shear wall, a foundation beam, slabs and piles, and to establish more rational design procedures for each structural component. The experimental parts of this study were already submitted to this report last year. With macro model of this specimen, the restoring force characteristic of the shear wall was predicted and damage evaluation of the foundation beam under the multi-story shear wall was conducted. This analytical study was performed by Masanobu SAKASHITA, Susumu KONO, Hitoshi TANAKA and Fumio WATANABE.

(2) Specimens

The specimen configuration was determined from typical fourteen-story residential buildings in Japan. The assemblage consisting of the lowest three floors of a shear wall with a foundation beam, the first floor slab, and two piles in the transverse direction was scaled to 1/4. Figure 10 shows specimen configuration.

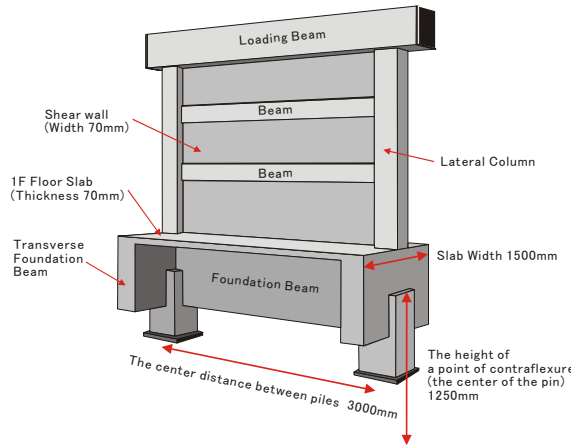


Fig.10 Specimen configuration

(3) Test Setup

As shown in Figure 11, lateral load, Q , was applied statically through a 1000kN horizontal jack to the loading beam. Two 2000kN vertical jacks were adjusted to create appropriate column axial forces, N_1 and N_2 , which are a liner function of lateral load, Q , to

simulate loading conditions of the prototype fourteen-story shear wall system under earthquakes. At the roller support, $0.7Q$ was applied horizontally to the pile on the compressive side and $0.3Q$ was applied to the piles on the tensile side by a 1000kN jack in the opposite direction to the 1000kN horizontal jack.

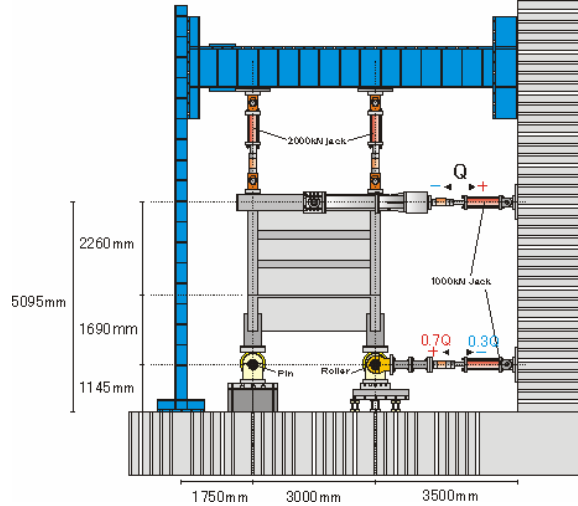


Fig. 11 Loading system

(4) Macro Model

Figure 12 shows macro model of this specimen. Shear wall was modeled based on Suzuki et al's study in 1993 and Miki et al's study in 2002. Columns and beams were modeled with rigid bodies, axial and shear springs. The angle of the concrete strut was fixed to be 45 degrees. Because this specimen failed in flexure, these struts were modeled to be elastic and not able to transfer tensile axial force. As to longitudinal bars of column, beam and foundation beam, the effect of the tension stiffening was considered using the model of Maekawa et al. (1999).

(5) Restoring Force Characteristic and Deformation Shape

Figure 13 shows Lateral load – 1F Drift angle relationship of the shear wall. Analyses were performed by two different methods. One method was conducted with shear wall-foundation model shown in Figure 12. The other method was conducted with shear wall model. This model has the same shear wall as shear wall-foundation model, but doesn't have the foundation beam and the base of the shear wall was fixed to the ground. Analytical results of shear wall-foundation model agreed with the experimental envelope curve.

Figure 14 shows deformation shape of shear

wall-foundation model when drift angle was 0.30%. Due to rotation of the compressive pile involving the transverse foundation beam, deformation of the compressive column of the shear wall was supposed to be smaller than that in case of using fixed shear wall base.

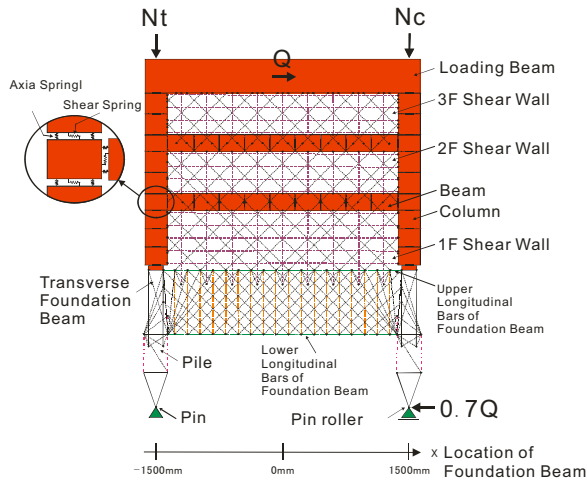


Fig. 12 Macro model

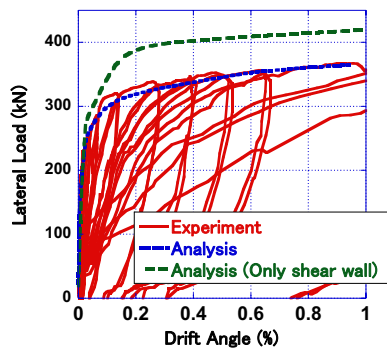


Fig. 13 Lateral load – first story drift relation

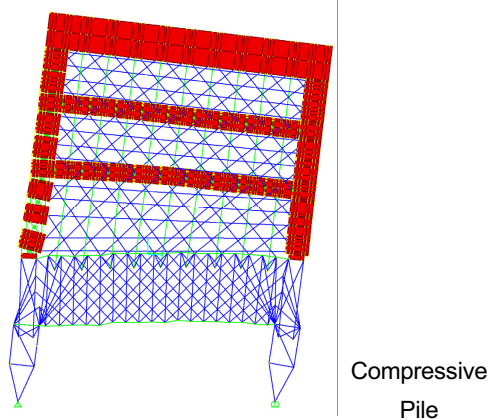
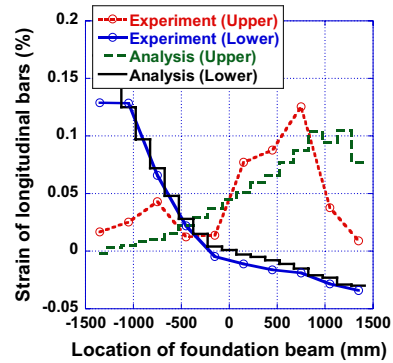


Fig. 14 Deformation shape of macro model (Drift Angle= 0.30%)

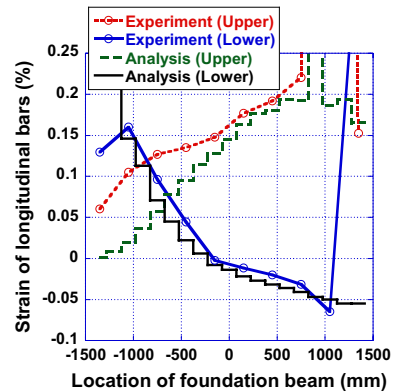
(6) Strain distribution of longitudinal bars of foundation beam

Figure 15 (a) (b) show strain distribution of longitudinal bars of foundation beam when flexural drift angle = 0.046% and 0.20%. Transition of the damage of the foundation beam was confirmed in experiment according to the flexural deformation of the shear wall above the foundation beam. This model simulates well the transition of the strain distribution of the upper and lower longitudinal bars of the foundation beam.



Drift Angle, Flexural Drift Angle, Lateral Load
Experiment (0.132%, 0.046%, 320.6kN)
Analysis (0.168%, 0.046%, 314.6kN)

(a) Relationship 1



Drift Angle, Flexural Drift Angle, Lateral Load
Experiment (0.637%, 0.203%, 354.8kN)
Analysis (0.815%, 0.203%, 361.1kN)

(b) Relationship 2

Fig. 15 Strain distribution of longitudinal bars of foundation beam

(7) Conclusions

One 1/4-scale cantilever structural wall system was tested and comparison was conducted with experimental results and analytical results based on strut-and-tie theory. The main conclusions can be summarized as follows.

1) The envelope curve of the load-drift angle

relationship was simulated well with the macro model including the foundation.

2) Transition of the strain distributions of the longitudinal bars of the foundation beam in experiment was simulated well.

4.2 Effects of Earth Pressure and Sidewall Friction on Pile Stress during Soil Liquefaction

(1) Objectives

This study is intended to: 1) examine the effects of liquefied soil layer on development of earth pressure and sidewall friction acting on an embedded footing in non-liquefied crust; and 2) investigate the effects of total earth pressure and sidewall friction on the shear force at pile heads. For those purposes, dynamic centrifuge tests on a superstructure-footing model that is supported on piles in either dry sand or in saturated liquefiable sand were performed.

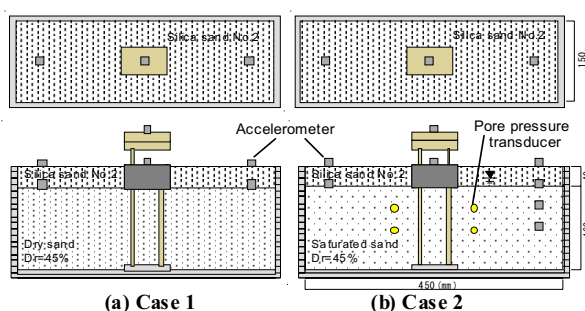


Fig. 16 Setup for centrifuge tests

(2) Model Preparation

Centrifuge tests were performed at 40 g centrifugal acceleration using the geotechnical centrifuge at the Disaster Prevention Research Institute, Kyoto University. A pile-footing-superstructure model was prepared in a laminar shear box with inner dimensions of 450 mm (length) \times 150 mm (width) \times 200 mm (height). Two cases of the performed tests are presented in Fig. 16. The soil profile in Case 1 consists of a 4.0 cm layer of dry coarse sand crust, which is Toyo silica sand #2 ($D_{50}=1.92$ mm) overlying a 16.0 cm layer of dry fine sand deposit, which is Albany silica sand #48 ($D_{50}=0.29$ mm). The soil profile in Case 2 resembles that of Case 1, except that the fine sand deposit is saturated and the water level was located at G.L. -3.0 cm. A viscous fluid made of Metolose (Shin-Etsu Chemical Co.), which has a

viscosity of 40 times that of water, was used.

A sketch and conditions of a piles-footing-superstructure model is shown respectively in Fig. 17 and Table 1. A 2×2 pile model was used for the tests. The lid-shaped footing was modeled with rigid brass. The pile heads were linked rigidly to the upper plate of the footing; their tips were also rigidly linked to the laminar shear box. The strain gauges at the pile heads were not in contact with the soil. Therefore, the shear force at the pile head, as calculated by the strain differentiation, was inferred to have been measured accurately, and independently of the soil effects. Plates supported by three load cells were set up on the right and left sides of the footing to evaluate earth pressure acting on the footing. The surface of the footing model is smoother than that of a prototype. Therefore, a fine grade of sandpaper #800 was pasted on the right and left sides and sidewalls of the footing. The superstructure was modeled with rigid brass. The mass

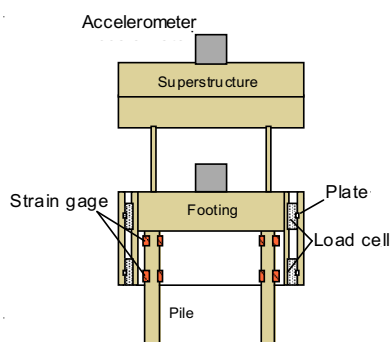


Fig. 17 Pile-footing-superstructure model

of the superstructure was 1.035 kg; that of the footing was 0.715 kg. The natural frequency of the superstructure under the fixed footing conditions was about 100 Hz. All tests were excited using Rinkai92, which is a synthesized ground motion for the Tokyo Bay area. All data presented in the following sections are of prototype scale.

(3) Effects of Earth Pressure and Sidewall Friction on Shear Force at Pile Head

Figures 18 and 19 show the time histories of the superstructure-footing inertia defined by the sum of the superstructure inertia and footing inertia, and the sum of shear force at the pile heads. The shear force at the pile heads is similar in waveform to the superstructure-footing inertia in the non-liquefaction test. Contrastively, the shear force differs greatly in

waveform from the superstructure-footing inertia in the liquefaction test. The shear force amplitude increases

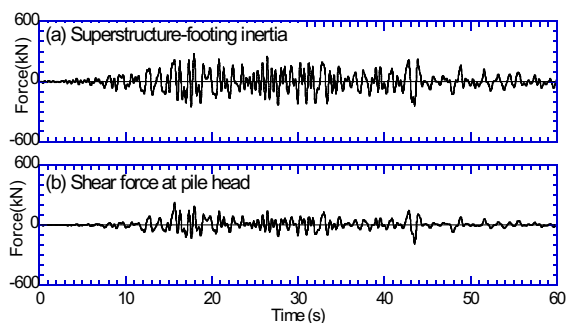


Fig.18 Time histories of superstructure-footing inertia and shear force at pile head in Case 1

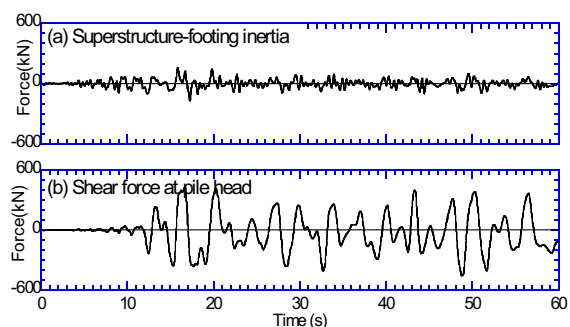


Fig. 19 Time histories of superstructure-footing inertia and shear force at pile head in Case 1

rapidly after time $t=10$ s. It is noteworthy that the shear force amplitude in the liquefaction test is greater than that in the non-liquefaction test, although the superstructure-footing inertia amplitude in the liquefaction test is less than that in the non-liquefaction test.

To elucidate the difference in the shear force between Cases 1 and 2, Fig. 5 shows the time histories of the superstructure-footing inertia, the sum of the total earth pressure and sidewall friction, shear force at the pile heads, soil displacement, and footing displacement for time $t=20-30$ s. In the non-liquefaction test, the sum of the total earth pressure and sidewall friction tends to be out of phase by 180 degrees with the superstructure-footing inertia and has smaller amplitude than the superstructure-footing inertia. Such tendencies indicate that the sum of the total earth pressure and sidewall friction, which are generated as reaction forces of the superstructure-footing inertia, counter the inertial force transmitted from the superstructure-footing to the pile head. Therefore, the shear force amplitude is less than

that of superstructure-footing inertia. The amplitude of footing displacement tends to be greater than that of soil displacement, suggesting that the total earth pressure and sidewall friction act on the footing as reaction forces.

Table 1 Conditions of piles-footing-superstructure model in prototype and model scale

	Unit	Prototype	Model
Pile	Diameter	m	0.24
	$E \cdot I$	MNm ²	30.72
Footing	Mass	kg	45,760
	Length (L×B×H)	m	3.20×2.00×1.72
Structure	Mass	kg	66,240
	Natural frequency	Hz	2.5
			100

In Case 2, the amplitude of the sum of the total earth pressure and sidewall friction tends to be greater than that of superstructure-footing inertia. The shear force resembles the sum of the total earth pressure and sidewall friction in waveform, which indicates that the shear force is caused mainly by the total earth pressure and sidewall friction. The amplitude of soil displacement tends to be greater than that of footing displacement, suggesting that the total earth pressure and sidewall friction act on the footing as external forces.

(4) Conclusion

The liquefied layer under the non-liquefied crust affects not only the superstructure-footing response but also the earth pressure and sidewall friction. The amplitudes of the total earth pressure and sidewall friction in liquefaction test are much greater than those in non-liquefaction test. In addition, the total earth pressure and sidewall friction in liquefaction test tend to be in phase with the superstructure-footing inertia. Consequently, the shear force amplitude at the pile heads becomes large. In non-liquefaction test, the total earth pressure and sidewall friction, generated as reaction forces of the superstructure-footing inertia, counter the inertial force transmitted from the superstructure-footing to the pile head. Therefore, the amplitude of shear force is smaller than that of superstructure-footing inertia.

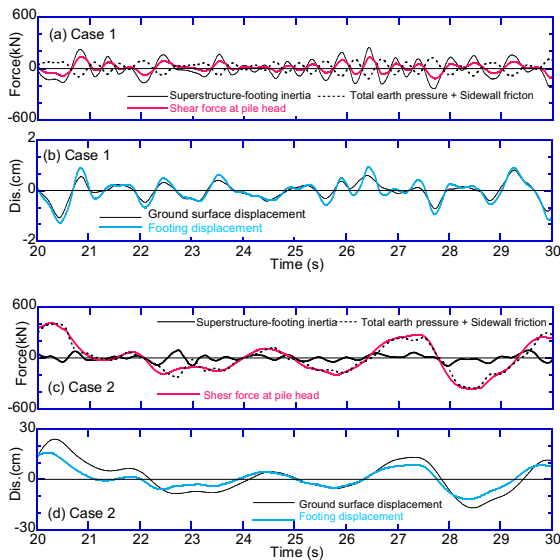


Fig.20 Time histories of superstructure-footing inertia, sum of total earth pressure and sidewall friction, and shear force at pile head in Cases 1 and 2

5. Development of Sloshing Reduction Dumper for Petroleum Tank with Floating Roof

5.1 Introduction

During 2003 Tokachi-oki earthquake, large amplitude of sloshing occurred in many petroleum tanks, and caused severe damage and fire. We will have the similar damage during Tokai, Tonakai and Nankai earthquake which are predicted to occur within 30- 50years. To reduce sloshing for petroleum tanks with floating roofs we propose a damper which consists of a separating wall with slits installed in the tank. We perform shaking table experiments to examine its effect on reduction of sloshing.

5.2 Model

The model used in the experiment is made of acryl cylinder whose diameter is 512mm, height 310mm, as shown in Fig. 21 and Photo 1. White colored water is used for measuring its surface by a laser gap sensor. The separation wall, which consists of stainless steel frame and brass panels, is installed in the model tank as shown in Fig. 21. 21 cases of panel layout, shown in Fig. 22, are examined in this study. The black area indicate the brass panels and the white area is open. The open ratio, α , is used to represent characteristics of the panel layout. Input motion is one directional sinusoidal wave with the frequencies from 1 Hz to 3

Hz (3.2 Hz in some cases), whose displacement is manually controlled to keep 1 mm. The height of liquid surface is measured near outer wall of cylindrical model tank, and recorded for 15 sec with 200 Hz sampling frequency. Note that effect of floating roof is not considered.



Photo. 1 Shaking Table Experiment

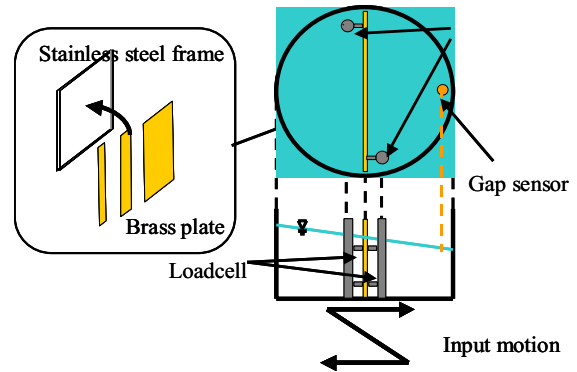


Fig. 21 Experimental Model

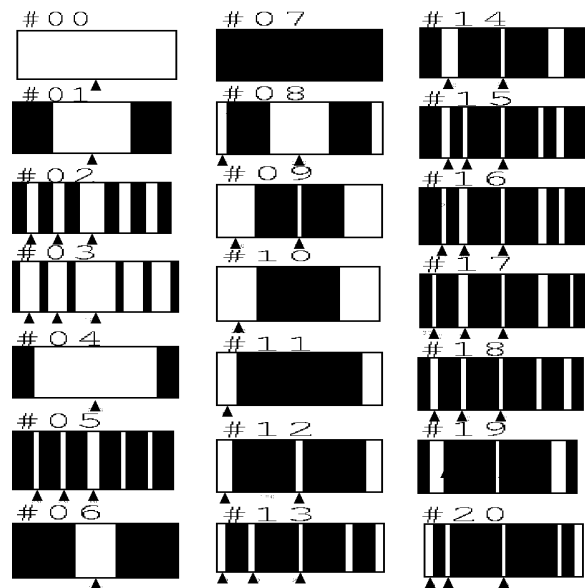


Fig. 22 Panel arrangement experimented

5.3 Effect on Reduction of Sloshing

Fig. 23 compares the non-dimensional frequency response function of sloshing height, that is divided by the displacement of input sinusoidal wave, in case #00 and case#07 which are the case with no separation wall ($\alpha=100\%$) and full separation wall ($\alpha=0\%$). In the case #00 we can recognize clear peaks at 1.2 Hz and 2.2 Hz which represent 1st mode and 2nd mode natural frequencies. Note that the peak value of 1st mode reaches 50 and that of 2nd mode is 20. It should be the reason why large sloshing occurs during earthquakes. In case #07, the peak at 1st mode disappears and new two peaks at 1.7Hz and 2.5Hz appear. These new peaks are generated because the tank is completely separated into two half parts and 1st mode and 2nd mode for the half part are excited. We call those modes “1.5th mode” and “2.5th mode” here after.

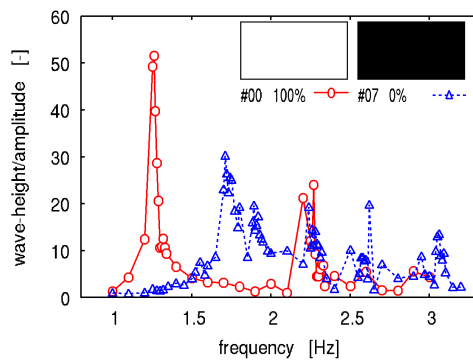


Fig. 23 Response Function (#00 and #07)

Fig. 24 shows the open ratio of the panel layout on the separation wall affects the response function. We find that small open ratio results small sloshing height at 1st mode and enlarge the 1.5th mode. On the other hand 2nd mode and 2.5th mode are not significantly changed.

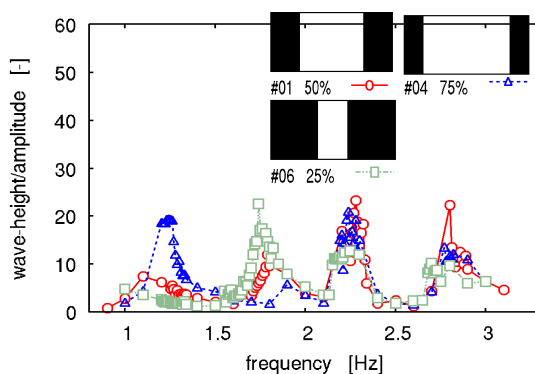


Fig. 24 Response Function (#01, #04 and #06)

To reduce the sloshing height during earthquakes, response values at 1.5th mode and 2.5th mode are also important as well as 1st mode. Fig. 25 shows the response function for cases #11 and #06 which have the same 25% open areas at different position on the separation wall. The figure implies that open area in the center of the wall reduces the sloshing height at 1.5th mode.

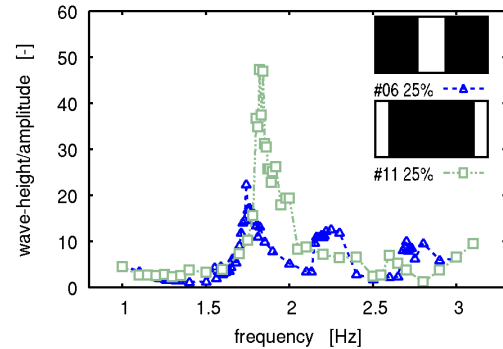


Fig. 25 Response Function (#11 and #06)

From the experimental results of other cases shown in Fig.21 we find that the layout with many small open area reduces the sloshing height at 2nd and 2.5th mode. We finally find that case #16 is the best case in the 21 cases experimented, which have small sloshing height through the wide frequency range. Fig. 26 shows the response function of case #16 in comparison with case #00, that is the case of no separation wall. Sloshing height at 1st mode reduced from 50 to 10. the height at 2nd mode also decreased from 20 to 10. On the other hand, 1.5th mode and 2.5th mode are newly excited while these heights are controlled to be about 10.

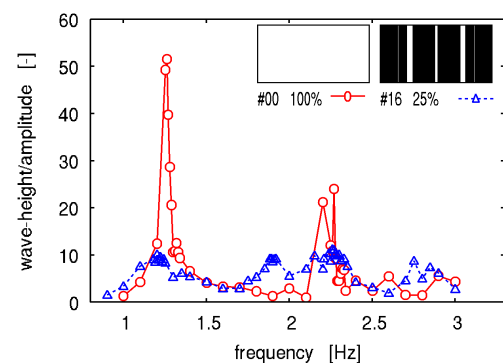


Fig. 26 Response function for the best case (#16) and no separation wall case (#00)

5.4 Conclusion

We propose a damper which consist of separation wall with slit installed in cylindrical tank in order to reduce the sloshing height during earthquake. Model

experiment is performed to examine its effect.

Small open ratio of the separation wall resulted small sloshing height at 1st mode while new modes, 1.5th mode and 2.5th mode, are excited because the tank is divided into 2 parts by the separation wall. 1.5th mode decrease if we open the center position of the separation wall and 2nd and 2.5th modes are reduced if the wall has many small open areas. We find the best layout of the separation wall from 21 experimental cases whose normalized sloshing height is restricted less than 10 in the wide frequency range.

6. Summary

We have conducted research study on precise evaluation of vulnerability of urban infrastructure against strong ground motions. Earthquake hazard in Japan is very high and the hypothetical Nankai subduction earthquakes will occur in near future. Integration of multiple evaluation indexes of seismic vulnerability for urban area is continuously important issue for seismic disaster mitigation. Cooperation studies of science and technology researchers should be continued.

Acknowledgements

We used K-NET, KiK-net, and CEORKA strong motion data.

References

- Architecture Institute of Japan: AIJ Standard for Structural Calculation of Reinforced Concrete Structures Based on Allowable Stress Concept, pp.218-241, 1999 (in Japanese).
- The Headquarters for Earthquake Research Promotion, On the long-term evaluation of earthquakes in the Nankai trough, http://www.jishin.go.jp/main/chousa/01sep_nankai/index.htm, 2001a (in Japanese).
- The Headquarters for Earthquake Research Promotion, The interim report on strong ground motion evaluation methods for projected earthquakes in the Nankai trough, <http://www.jishin.go.jp/main/kyoshindo/01b/index.htm>, 2001b (in Japanese).
- Irikura, K., Prediction of strong acceleration motions

- using empirical Green's function, *Proc. 7th Japan Earthq. Eng. Symp.*, pp.151–156, 1986.
- Japan Meteorological Agency, *On Seismic Intensity*, Gyosei, Tokyo, 238 pp., 1996 (in Japanese).
- Kamae, K., Source modeling of the 2005 off-shore Miyagi prefecture, Japan, earthquake (M_{IMA}) using the empirical Green's function method, *Earth Planets Space*, **58**, pp.1561–1566, 2006.
- Lee, T. H., Kato, M., Matsumiya, T., Suita, K., and Nakashima, M., Seismic Performance Evaluation of Non-Structural Components: Drywall Partitions, *Earthquake Engineering and Structural Dynamics*, **36**, pp.367-382, 2007.
- Maekawa, K. and N. Fukuura, Re-Formulation of Spatially Averaged RC Constitutive Model with Quasi-orthogonal Bi-directional Cracking, *Journals of the Japan Society of Civil Engineers* No.634/V-45, pp.157-176, 1999 (in Japanese)
- Miki, T., M. Lertsamattiyakul, and J. Niwa, Numerical Evaluation for Flexural Deformation of Reinforced Concrete Columns Subjected to Axial and Flexural Loads Using Lattice Model, *Transactions of the Japan Concrete Institute 2001*, **23**, pp.231-238, Feb. 2002.
- Okada, T., T. Yaginuma, N. Umino, T. Kono, T. Matsuzawa, S. Kita, and A. Hasegawa, The 2005 M7.2 MIYAGI-OKI earthquake, NE Japan: Possible rerupturing of one of asperities that caused the previous M7.4 earthquake, *Geophys. Res. Lett.*, **32**, L24302, doi:10.1029/2005GL024613, 2005.
- Okamura, H. and K. Maekawa: Nonlinear Analysis and Constitutive Models of Reinforced Concrete, *Gihoudo-Shuppan*, 1991.
- Paulay, T. and M.J.N. Priestley, Seismic Design of Reinforced Concrete and Masonry Buildings. *John Wiley & Sons*, pp.362-499, 1992.
- Suzuki, S. et al., Elasto-Plastic Analysis of Framed Shear Walls Subjected to Alternately Reversible Horizontal Force Using Macro Model, *Summaries of Technical Papers of Annual Meeting Architectural Institute of Japan*, pp.307-308, 1993 (in Japanese).
- Suzuki, W., T. Iwata, K. Asano, and N. Yamada, Estimation of the source model for the foreshock of the 2004 off the Kii peninsula earthquakes and strong ground motion simulation of the hypothetical Tonankai earthquake using the empirical Green's

function method, *Earth Planets, and Space*, **57**, pp.345-350, 2005.

Wu, C., and K. Koketsu, Source process of the 2005 and 1978 Miyagi-ken Oki earthquakes inverted

from strong motion records, *Seism. Soc. Japan, Fall Meeting*, Abstract PM20, 2005.

多次元指標の統合化による都市施設地震脆弱性診断手法の高度化

中島正愛・田中仁史・岩田知孝・澤田純男・田村修次

要 旨

都市域に存在する多くの構造物の地震時における脆弱性を合理的に評価して危険度を低下させるための取り組みを、入力地震動評価の高度化、地盤・基礎の相互作用や非構造部材の応答特性に関する詳細な分析、長周期地震動による大型タンクスロッシング被害の軽減方策に関する各研究をすすめた。これらの各要素の結合により都市施設の地震時脆弱性の評価とそれに基づく防止対策を推進することができる。

キーワード： 強震動，非構造部材応答，地盤構造基礎相互作用，スロッシング低減ダンパー